Physics of Plasmas ARTICLE scitation.org/journal/php

Re-entry blackout elimination and communication performance analysis based on laser-plasma-induced X-ray emission

Cite as: Phys. Plasmas **26**, 033503 (2019); doi: 10.1063/1.5056210
Submitted: 13 September 2018 · Accepted: 17 February 2019 ·
Published Online: 5 March 2019

Huan Li,[1,2] Xiaobin Tang,[1,3,a)] Shuang Hang,[1] Yunpeng Liu,[1,3] Junxu Mu,[1] and Wei Zhou[1]

AFFILIATIONS

[1]Department of Nuclear Science and Engineering, Nanjing University of Aeronautics and Astronautics, Nanjing 211106, China
[2]Institute of Laser Engineering, Osaka University, 2-6 Yamada-oka, Suita, Osaka 565-0871, Japan
[3]Key Laboratory of Nuclear Technology Application and Radiation Protection in Astronautics, Nanjing University of Aeronautics and Astronautics, Nanjing 211106, China

[a)]**Author to whom correspondence should be addressed:** tangxiaobin@nuaa.edu.cn. Tel.: +86 13601582233. Fax: +86 025 52112908-80407.

ABSTRACT

X-ray communication (XCOM) offers important advantages to both civilian and military space projects. Rapid advance in high-intensity laser interaction with plasma has become a driving force for providing a new X-ray carrier generation based on the laser wakefield acceleration scheme. XCOM has the potential to eliminate RF shielding on the ground and communicate with the re-entry supersonic spacecraft during blackout occurrence. In this process, the plasma sheath is formed around the surface due to air compression and ablation, which blocks the traditional communication signals. In this paper, the hazardous substance was proactively exploited and coupled with the modulated laser. Particle-In-Cell simulation results indicate the ultra-bright controllable X-ray emission with a small angular divergence (0.04 rad × 0.03 rad), a tunable X-ray energy range (4.60 keV to 321.48 keV), and high photon yields. Additionally, the data rate of the communication via the X-ray carrier during re-entry was estimated up to ∼20.7 Mbps by considering the transmission model, encoding schemes and photon information efficiency. Combined with an existing or developing X-ray detection technique, this regime can eliminate re-entry blackout and also provide a novel modulated X-ray source to acquire high-rate, low transmit power, and highly secure space-based data links.

I. INTRODUCTION

High-demanding data rates in fiber-optical and free-space optical wireless communication have been exponentially increasing over recent decades.[1] X-ray communication (XCOM), which was first proposed by Dr. Keith Gendreau, is known as one of the most promising revolutionary concepts by NASA in fast wireless link technology since 2007.[2] The data transfer rate of the X-ray link with the 3.0×10^{10} GHz range can reach 40 Petabits/s using on-off keying (OOK) modulation theoretically.[3] XCOM technology exploits extremely low beam divergence and high photon yields of X-rays with a tunable energy range, which can provide high-rate, deep-space, low transmit power, and highly secure space-to-space data links.[2]

NASA displayed the world's original XCOM system using a modulated X-ray source with the intention to increase the data rate from 50 kbps to 1 Mbps.[4] Kealhofer *et al.* illustrated an ultrafast X-ray point source for space-based communications exploiting laser-triggered X-ray emission from hafnium carbide tips.[5] XCOM opens novel research horizons with countless applications, including high-speed interplanetary communication, secure short-range communication, and X-ray navigation.[2] To adopt X-rays for terrestrial applications, higher X-ray energies are required. The penetrating capabilities of X-rays with higher energies enable the communication possibility during hypersonic spacecraft re-entry into the planetary atmosphere. In this process, a plasma sheath is formed around the spacecraft surface due to the dissociation and ionization of neutral particles by shock wave heating. However, the plasma sheath will attenuate or reflect the traditional RF signals and prevent the normal telemetry transmission, which causes re-entry blackout.[6–10] Although current alternatives for blackout mitigation have been excessively investigated (including the $\boldsymbol{E} \times \boldsymbol{B}$ layer,[6] frequency matching,[8] and injection of electrophilic material[9] methods), no satisfactory solutions have been established. In addition, inflatable aeroshell technology[10] was also proposed for mitigating

blackout communication during spacecraft reentry. In our previous work,[11] we discovered that XCOM is suitable for plasma sheath environments, and various plasma electron densities have no significant effect on the bit-error-rate (BER) performance of XCOM at a similar signal-to-noise-ratio (SNR) of the same receiver due to the high X-ray carrier frequency.

The exceedingly high carrier frequency of X-rays provides significantly large bandwidths for information transmission if technology for modulating the X-ray source is further developed. Most of the existing X-ray modulated sources for XCOM are bremsstrahlung-based emission. Although a conventional X-ray tube is a cheap and flexible source for this application, the extremely low conversion efficiency from the accelerated electrons to the emitted X-ray photons (~1%) with a large photon beam divergence and low radiation brilliance will limit its application in this sophisticated field. As reported in the existing literature, the data rate of XCOM is very slow with ~kbps order.[4] Therefore, it is necessary to employ new modulated X-ray emission technology for communication. Fortunately, chirped pulse amplification (CPA)[12] technology helps the current commercial high-power laser system to deliver peak powers up to petawatt, which can be focused to realize laser intensities ranging from 10^{15} to 10^{21} W/cm^2. With the advent of tabletop ultrashort and ultra-intense modulated lasers, the laser wakefield acceleration (LWFA) scheme proposed by Tajima and Dawson[13,14] has demonstrated considerable potential in producing ultra-bright X-rays with high photon yields, a well-collimated beam, and a tunable X-ray energy range. Together with an existing electro-optic modulator[15] or an advanced plasma optical modulator,[16,17] the transmission signal would be easily modulated with X-rays to realize high-rate communication.

In this paper, we proposed a new X-ray generation regime to realize real-time blackout communication by exploiting the modulated laser interaction with the plasma sheath during spacecraft re-entry. In general, the plasma sheath acts as the hazardous substance hampering real-time communication. The scheme we propose here makes full use of this complicated plasma sheath as an available substance to generate X-ray carriers. The schematic diagram of the regime for mitigating blackout is shown in Fig. 1. X-ray communication uplink and downlink between spacecraft and International Space Station (ISS) will be established depending on where the laser generator is located. X-ray links are from the spacecraft (transmitter) to the International Space Station (ISS, receiver) and then transfer data to the ground station for deep space communication and blackout communication. As an additional technology enhancement to the Station Explorer for X-Ray Timing and Navigation Technology (SEXTANT) mission, scientists at NASA are developing a follow-on technology demonstration of XCOM that will exploit the instrument as a passive receiver.[18] We expected that the laser generator will be placed inside the capsule in our scheme. Although the generator size will limit the practical application according to the current laser facilities, rapid development in laser technology will be expected to make the ultra-intense laser possible and satisfy the demands of smaller generator size at the same time. In this scheme, a linearly polarized modulated laser propagates in an underdense plasma sheath around the spacecraft surface. The ponderomotive force of laser pulses and the relativistic increase in the electron mass modify the refractive index of the plasma, which generates laser pulse self-channeling in plasma and extends the propagation distance of the laser. Meanwhile, the plasma electron motion induces positive and negative charge separation fields behind the laser pulse which

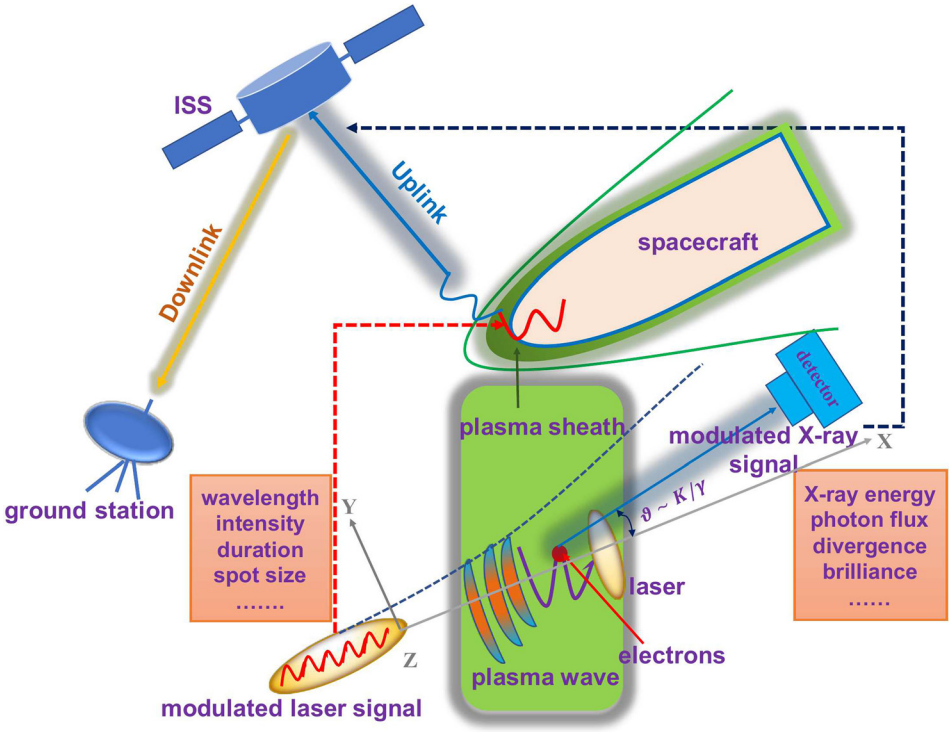

FIG. 1. Schematic diagram of the laser-plasma X-ray generating scheme used for mitigating blackout communication during re-entry, where X-ray links are from the spacecraft (transmitter) to the International Space Station (ISS, receiver) and then transfer data to the ground station.

results in high accelerating electric fields and a strong restoring force that drives the oscillation of plasma electrons, thereby generating directional high-quality X-ray radiation.[19–21] In this paper, we covered the topics related to the modulated laser-plasma-induced X-ray emission performances (the photon yields, small angular divergence, and tunable energy range) and accelerated electron beams by 2D-Particle-In-Cell (PIC) simulation, followed by a detailed description of the data rate of the XCOM system during re-entry by considering the transmission model, encoding scheme, and photon information efficiency (PIE).

II. THEORIES AND METHODS

The 2D EPOCH PIC simulation[22] was employed to study the modulated laser interaction with the plasma sheath. The simulation was carried out with a box that is $X \times Y = 45\,\mu m \times 40\,\mu m$ and sampled by 900×430 cells with 50 macro-particles in the longitudinal and transverse directions. Moving-window technology was employed and started to move once the front of the laser was 0.9 on its way through the box, which was parallel to the x direction at the group velocity of light in vacuum. The technology was used for keeping the track of the evolution of the laser, laser wakefield-accelerated electrons, and X-ray emissions on different transmission timings. The wakefield was driven in a fully ionized nitrogen and oxygen plasma using laser pulse with the following Gaussian envelope:

$$a(t,y) = a_0 \exp\left(-\frac{y^2}{w_0^2}\right)\exp\left(-\frac{(t-\tau_0)^2}{\tau_0^2}\right), \tag{1}$$

where $a_0 = 4.0$ is the peak strength corresponding to a laser intensity of $I_0 = 1.37 \times 10^{18} a_0^2/\left[\lambda_0(\mu m)\right]^2 = 3.34 \times 10^{19}\,W/cm^2$ with a laser wavelength of $\lambda_L = 0.81\,\mu m$. It is useful to define a normalized peak vector potential of $a_0 = eA_0/(mc) = eE_L/(mc\omega_0)$, where A_0 is the vector potential; E_L and ω_0 denote the amplitude of the electric field and angular frequency of the laser beam. $\tau_0 = 40$ fs is the full width at half maximum (FWHM), and $w_0 = 10\,\mu m$ is the $1/e^2$ focal spot size and focuses on the front surface of plasma. In addition, the re-entry plasma sheath electron density is non-uniform and strongly related to the shape, velocity, trajectory, angle of attack, and altitude of the spacecraft. In our previous study, we discovered that the plasma sheath distribution outward from the surface of the spacecraft (stagnation region) can be expressed by using the following double Gaussian function:[23]

$$n_e(x) = \begin{cases} n_{emax}\exp\left(a_1(x-x_0)^2\right) & (0 \le x \le x_0) \\ n_{emax}\exp\left(-a_2(x-x_0)^2\right) & (x_0 \le x \le x_1), \end{cases} \tag{2}$$

where n_{emax} is the peak value of the plasma electron density, x_1 is the thickness of the plasma sheath, x_0 is the location of the boundary layer, and a_1 and a_2 represent normal distribution's shape. The electron density of the plasma sheath[7] in the stagnation region varies from a few electrons/cm^3 to 10^{18} electrons/cm^3. We set the parameters of $n_{emax} = 5.0\times10^{-3} n_{cr} \sim 10^{18}\,cm^{-3}$ (n_{cr} represents the critical plasma density at which the plasma frequency equals the frequency of an electromagnetic wave in a plasma. It is given by $n_{cr} = \varepsilon_0 m_e \omega^2/e^2$. If the plasma density is lower than critical density, it will be called underdense plasma.), $a_1 = 1$, $a_2 = 0.5$, $x_0 = 0.4$ cm, and $x_1 = 1$ cm in the simulation, according to the typical values of the re-entry plasma sheath generated by the NASA Langley Research Center.[7,24] For the laser-plasma X-ray scheme, the X-ray radiation is generated in the wake of the laser and plasma interaction, which is also the advantage of the laser wakefield acceleration regime. However, large-scale laser plasma simulation is an increasingly demanding area of computational physics. Therefore, we employed the thickness of the plasma sheath of 1 cm. The laser pulse was launched into the double Gaussian plasma in the x-direction and linearly polarized in the y-direction. In Secs. III and IV, the electron number density evolution, X-ray photon angular divergence, and energy spectrum in laser interaction with plasma will be discussed through 2D-PIC simulation. Potential blackout alleviation and the data rate of the emitted X-ray carrier based on the PIC results during re-entry will be elucidated in detail.

III. RESULTS AND DISCUSSION

A. Modulated laser interaction with the plasma sheath during re-entry

In this section, we first clarified the potential problem of exploiting self-guiding laser communication in the plasma sheath and then provided a detailed description of effective X-ray communication in mitigating blackout based on laser interaction with the plasma sheath.

1. Pump depletion length of the laser through the plasma sheath

Poddar and Sharma[25] indicated that a relativistic self-focusing laser beam has been explored to mitigate the blackout problem and establish the communication link between the spacecraft and ground station as supersonic spacecraft enters the atmosphere if the power of the modulated laser P_L exceeds the critical power P_{cr} required for the plasma sheath[26]

$$P_{cr} = 16.2\left(\frac{\omega_0}{\omega_p}\right)^2 (GW), \tag{3}$$

where ω_0 and ω_p denote the angular frequency of the laser and the plasma sheath. On the one hand, the focusing and accelerating fields are not ideal, and it is difficult to obtain high efficiency in the stable self-guiding regime. On the other hand, as the self-focusing laser through the plasma sheath, it will be depleted after a distance (pump depletion length L_{pd}) due to its energy transfer and loss, and the pump depletion length is given by[27]

$$L_{pd} \simeq \frac{\omega_0^2}{\omega_p^2} c\tau_{FWHM}, \tag{4}$$

where ω_p and ω_0 represent the plasma frequency and the laser pulse frequency and τ_{FWHM} is the full width at half maximum (FWHM). The laser carrier will cause a series of nonlinear phenomena when it penetrates the plasma sheath around the spacecraft surface, which depends on laser diffraction, accelerated electron dephasing, the laser pump depletion length, and laser-plasma instabilities. Even in vacuum, a laser pulse undergoes Rayleigh diffraction as well, and the laser-plasma interaction distance will be limited to a few Rayleigh lengths $Z_R = \pi w_0^2/\lambda$ without any form of optical guiding.

In the simulation, all other parameters remained the same as in Sec. II. Although the modulated laser carrier could meet the needs of the self-focusing property with the power of the laser $P_L = 52.5$ TW

greater than the critical power $P_{cr} = 3.3$ TW, it would transfer its energy to the plasma sheath and became depleted after $L_{pd} = 0.49$ cm according to Eq. (4). As shown in Fig. 2, this is also supported by the PIC simulation results of L_{pd} which is about 0.46 cm at 15 ps, and the evolution plot of the normalized peak vector potential a_0 decreases from 4.0 to 0.43 when the laser pulse travels in the plasma, which transfers its energy to the plasma wave and then depletes. Therefore, the laser carrier cannot penetrate the plasma sheath (approximately 1 cm here), and blackout communication occurs inevitably during spacecraft re-entry. However, the concomitant generated X-ray photon in the LWFA scheme will have a potential advantage. In our previous studies,[11,23] the transmission coefficient of the X-ray carrier through a plasma sheath with various electron densities is closer to 1 by adopting Wentzel-Kramers-Brillouin (WKB) and Finite-difference Time-domain (FDTD) methods due to its extremely high frequency. Therefore, the concomitant generated X-ray carrier through laser interaction with the plasma sheath will display extensive perspectives in mitigating blackout communication during spacecraft re-entry.

2. X-ray communication carrier induced by laser interaction with the plasma sheath

During the laser interaction with plasma, X-ray betatron radiation is produced when relativistic electron beams are injected into the laser wakefield in a plasma and experience synchrotron-like betatron oscillations transversely while accelerated in a forward direction.[13] X-ray emissions based on the betatron radiation from laser wakefield-accelerated electrons have a small divergence angle, compact sizes, high photon flux, and a wide energy spectrum. X-ray stable output properties in the betatron radiation, such as photon flux, the photon energy spectrum, and angular divergence, are essential for an effective X-ray communication carrier, which depends on the stability of the accelerating structure's amplitude, wavelength, and phase velocity during the entire accelerating process. A stable bubble structure can be excited in the betatron radiation under the following matching condition:[27]

$$k_p w_0 = 2\sqrt{a_0}, \tag{5}$$

where k_p is the plasma wave number depending on the electron number density of the plasma sheath. Through adjusting the relation of the laser and plasma parameters from Eq. (5), the stable X-ray emissions will be generated. Intense betatron radiation, with photon energy from keV X-rays to gamma-rays, has been generated via the accelerated electrons undulating in the bubble structure of the wakefield. Therefore, in order to get the optimum X-ray emissions (X-ray energy range, divergence angle, etc.), a supersonic clustering gas jet[21] will be supplemented to increase the plasma electron number density in the relevant experiment. Figure 3(a) presents a stable bubble structure of the plasma density profile behind the laser pulse at $t = 2.3$ ps and 10 ps in the betatron radiation. On the one hand, the ponderomotive force of an intense laser pulse ($a_0 \geq 1$) expels the electrons of the non-uniform plasma sheath radially and leaves a bubble region due to the large ion mass. On the other hand, the attractive Coulomb force is exerted on the electrons causing them to flow backward to the rear of the bubble. As illustrated in Fig. 3(b), as the electron density at the bubble surface accumulates, the wave-breaking limit occurs and electrons are self-injected and accelerated inside the bubble. Then, the isotropic ponderomotive force in the transverse direction induces the isotropic oscillation of self-injected electrons, which further leads to the isotropic angular distribution of the betatron radiation. The betatron oscillations of the electron beam bunch in the transverse field of the bubble induce efficient X-ray generation, which shows a potential application in developing tabletop X-ray sources. Also, when the plasma sheath density, laser spot size, and laser peak intensity are inconsistent with Eq. (5), an unstable bubble structure emerges inevitably. However, the X-ray photon angular distribution of the betatron radiation is determined by the stability of the bubble structure. A stable bubble structure results in a small angular distribution of X-ray photons, which contributes to X-ray transmission signal detection as a communication carrier.

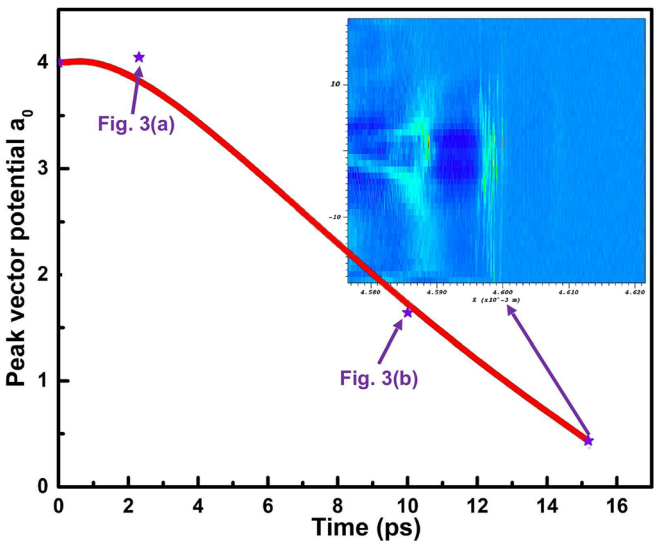

FIG. 2. Laser's normalized peak vector potential a_0 versus accelerating time evolution during laser interaction with the plasma sheath. The insets show the electron density evolution at 2.3 ps, 10 ps, and 15 ps. The laser pulse carrier depletes (a_0 decreases from 4.0 to 0.43), and the acceleration process terminates after the pump depletion length of 0.46 cm at 15 ps as it travels through a plasma sheath.

B. Angular distributions of X-ray for communication during re-entry

For XCOM application, the angular distributions of X-ray photons as communication carriers directly affect the effective signal transmission and communication coverage range. Therefore, several X-ray focusing methods have been proposed, such as mirrors,[28] zone plates,[29] and refractive lenses.[30] A well-collimated (small angular divergence) X-ray emission is produced through the laser pulse which propagates in an under-dense plasma. During this process, some electrons are injected into the laser wakefield in plasma and experience transverse betatron oscillations while being accelerated in a forward direction. Therefore, the angular divergence of the emitted X-ray photon in the laser transmission direction and the y-polarization direction was considered in this work. As illustrated in Figs. 3(c) and 3(d), the

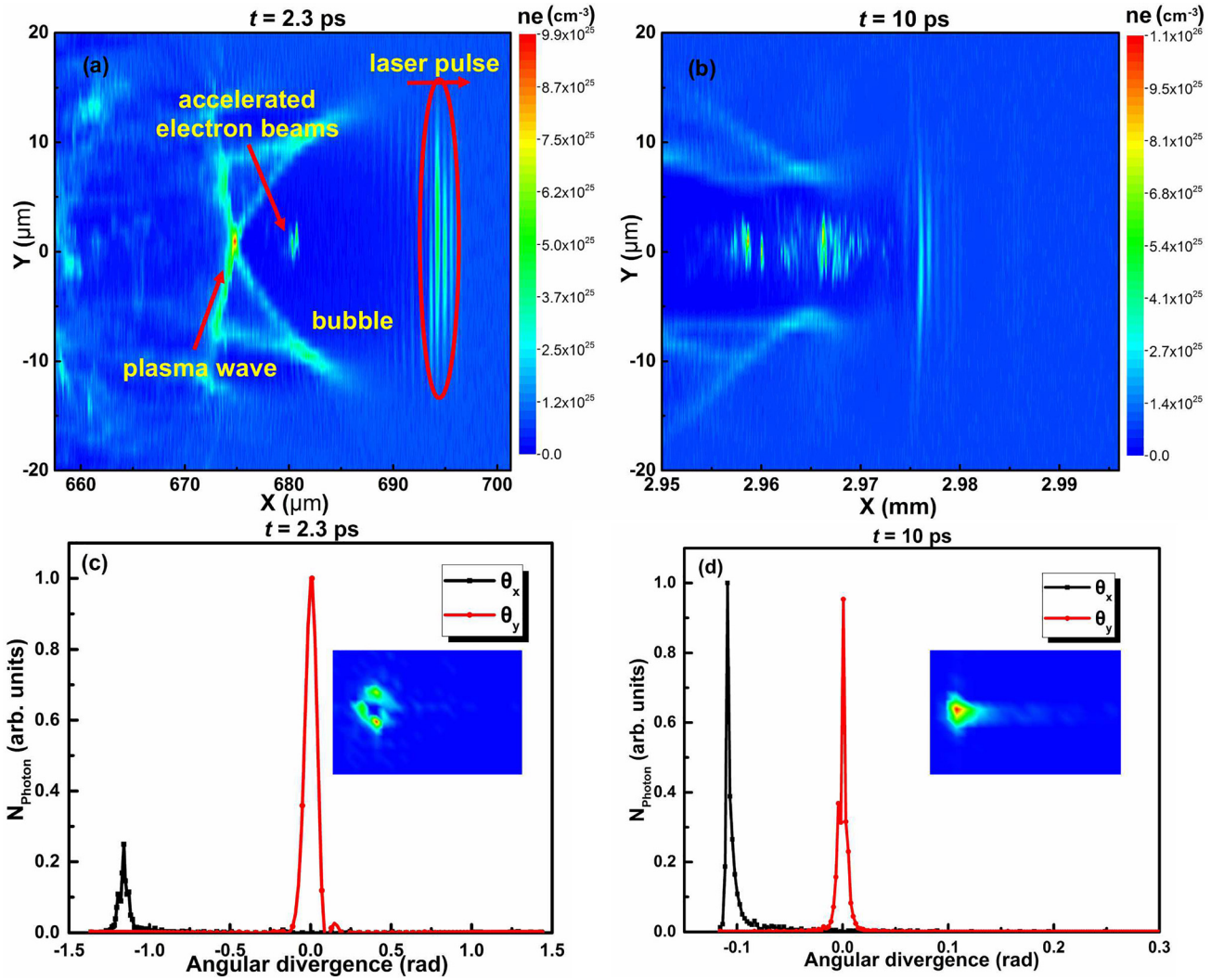

FIG. 3. Schematic diagram of the plasma electron density distributions behind the laser pulse in the betatron radiation. The radially expelled electrons flow backward to the rear of the bubble and collide in the x direction at the base of the bubble. The results show a stable bubble structure evolution at (a) t = 2.3 ps and (b) t = 10 ps. "Moving window" technology is employed in PIC calculations to keep track of the evolution of the laser, laser wakefield-accelerated electrons, and X-ray emissions on different transmission timings. After 10 ps, the laser travels to ∼3 mm (the plasma sheath thickness is 1 cm here); angular divergence of the emitted X-ray photon in the laser transmission direction and the y-polarization direction at (c) t = 2.3 ps and (d) t = 10 ps. Here, the angular divergence of a photon with a FWHM angle is defined as $\theta_y = \tan^{-1}(P_y/P_x)$, $\theta_x = \tan^{-1}(P_\perp/P_x)$, and $P_\perp = \left(\sqrt{P_y^2 + P_z^2}\right)$. The emitted photon numbers in different radiation directions are normalized by the maximum of the photon number. The insets show the distribution of emitted betatron photons in phase space (P_x, P_y), which is also good evidence to validate that most photons are forwardly emitted with low angular divergence.

obvious advantage of the regime we proposed here is that the emitted X-ray carrier has small angular divergence. In general, this is a common method in which the Gaussian function[31] fits the photons' angular distribution in the laser plasma interaction field by using the fitting function $f(\theta) \sim \exp(-\frac{\theta^2}{2\sigma^2})$. The photons are dominated in the forward direction and y polarization with a 50% energy spread (FWHM) angular divergence of 0.04 rad × 0.03 rad at 10 ps, corresponding to 2.3° × 1.7°. At the initial stage of 2.3 ps in the bubble acceleration, the photon angular divergence of 0.15 rad × 0.13 rad (8.6° × 7.5°) is slightly larger than that of the stable evolution process because of the large energy spread of the trapped electron beams inside the bubble.

In addition, the oscillations of the accelerated electrons induced by the bubble oscillations are along the *y* direction; hence, the photon angular divergence of the betatron radiation should also be anisotropic. The angular divergence of the emitted photons theoretically scales as $\theta_d = (n_e/a_0 n_{cr})^{1/3}$,[31] which could be adjusted by changing the laser pulse and plasma parameters. On the other hand, although the narrow X-ray beam-width creates a challenge in the acquisition,

tracking, and pointing accuracy (ATP) technology, it can be improved by incorporating other inertial guidance instruments and a beacon. The communication link among the ground terminal, spacecraft, and space terminal has been established by exploiting the combination of gimbal and actuators on the transmitting optics to maintain the pointing and tracking accuracy to 10 μrad with an angular coverage of 500 mrad.[32] The optical receiver comprises highly sensitive signal detectors which can convert the X-ray photons into electrical signals to recover the original transmission information by employing regular demodulation methods.

C. X-ray photon energy range for effective communication during re-entry

Our previous work has proved that employing an X-ray source with different energies according to the different spacecraft re-entry altitudes is imperative when using XCOM uplink or downlink to connect the communication with the spacecraft, International Space Station, and ground terminal.[11] Therefore, the energy of the emitted X-ray photons is also an important factor to realize the effective uplink or downlink communication for mitigating blackout.

In the laser-plasma interaction regime, the trapped electrons will be accelerated both longitudinally and wiggled transversally by the wakefield behind the drive laser pulse. The transverse motion is almost sinusoidal at the betatron frequency of $\omega_\beta = \omega_p/(2\gamma)$, where $\gamma = 1/\sqrt{1-(v/c)^2}$ is the Lorentz factor and $\omega_p = \sqrt{(n_e e^2/m_e\varepsilon_0)}$ is the plasma frequency. Because of the oscillatory motion of trapped electrons, the emitted photon radiation properties depend on the strength parameter $K = \gamma_\beta k_p\sqrt{\gamma/2}$ (γ_β is the betatron transverse amplitude of motion and k_p is the plasma wavenumber) and on the electron energy $E_e = \gamma m_e c^2$. The on-axis spectrum is almost monochromatic with only the fundamental frequency, which is well known as the undulator regime with $K \ll 1$. The wiggle regime occurs when $K \gg 1$, the spectrum contains many closely spaced and unresolved high harmonics, and the resulting broadband spectrum is extended up to a critical frequency of $\omega_c = 3K\gamma^2\omega_p/2$. Its envelope can be described by synchrotron-like radiation.[33] For a single electron with fixed parameters K, ω_β, and γ, the integrated radiation spectrum can be given by $dI/d\omega \propto S(x=\omega/\omega_c) = x\int_x^\infty K_{5/3}(\xi)d\xi$, which is similar to the synchrotron betatron spectrum, where $K_{5/3}$ is the modified Bessel function of the second kind.[34] The average photon numbers with the mean energy $\hbar\omega_c$ radiated by one electron can be estimated by $N = 5.6\times10^{-3}N_0K$, where N_0 is the number of betatron oscillations excited by the electron. Most present experimental data have demonstrated that laser-plasma betatron radiation occurs dominantly in the wiggler regime.[33,35]

To have a better understanding of the emitted X-ray properties based on laser-plasma interaction, PIC simulation was employed to calculate the radiation emitted by a single electron in the wiggle case, which can be simplified to the calculation of the sum of all kinds of radiations excited in N_p turning points of their sinusoidal trajectories as follows:

$$\frac{d^2I}{d\omega d\Omega} = \sum_{j=1}^{N_p}\left(\frac{d^2I}{d\omega d\Omega}\right)_j, \tag{6}$$

where ω is the photon frequency and $d\Omega$ is a solid angle.[36] In the simulation, the universal function $S(\omega/\omega_c)$ referred above defined that the relativistic electron emits along its momentum direction and an excited radiation spectrum at any given time. The EPOCH code extended by a particle tracker subroutine can be used for recording the trajectories of each electron and calculating the emission during the laser-plasma interaction. Figure 3(a) shows that electron self-injection into the ion cavity remains continuous. Therefore, the electron spectrum remains continuous as well, with the maximum energy of around 625.4 MeV at 10 ps shown in the inset in Fig. 4. Using the synchrotron distribution $S(\omega/\omega_c)$ defined above, we obtained a best fit for the critical energy of $E_c = \hbar\omega_c = 4.60$ keV as shown in Fig. 4. A significant feature of the scheme (laser interaction with the plasma sheath) is the presence of a broadband X-ray photon energy range in the betatron radiation, and the photon energy varies from 4.60 keV to the maximum 321.48 keV at 10 ps. In the LWFA regime, the photon energy E_{ph} can be expressed as[31]

$$a_f = a_0\left(\frac{n_e}{a_0 n_{cr}}\right)^{1/3}\left(\frac{\pi w_0}{\lambda_0}\right)^{2/3}, \tag{7}$$

$$E_{ph} \propto \hbar\nu_0 a_f^5\left(\frac{a_f n_{cr}}{n_e}\right)^2 n_{cr}\lambda_0^2 c^3\tau_0, \tag{8}$$

where a_f and w_0 denote the self-shaped and initial beam radii, respectively, ν_0 denotes the laser frequency, and $\hbar$ is the Planck constant. Therefore, the emitted photon energy E_{ph} could be adjusted by tuning the laser pulse and plasma sheath parameters, which would satisfy the demand for a tunable X-ray energy of XCOM in blackout communication during spacecraft re-entry in order to ensure an effective uplink or downlink communication.

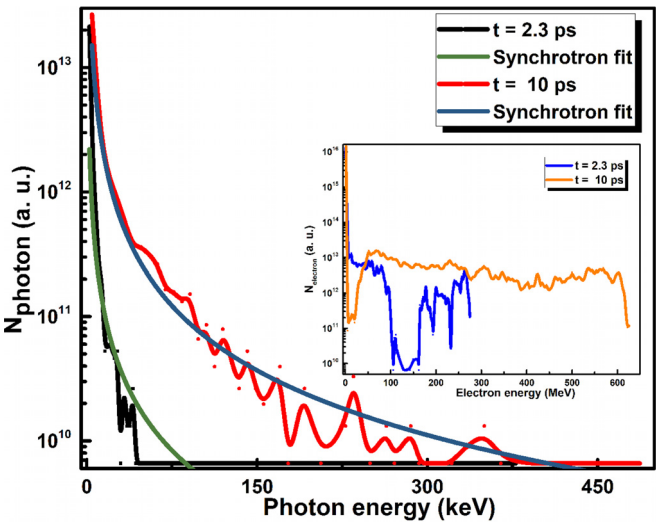

FIG. 4. Number of photons emitted from the betatron radiation (the energy spectrum of radiated photons) as a function of the radiated photon energy for a fixed laser amplitude of $a_0 = 4.0$ at the acceleration time of t = 2.3 ps (red) and t = 10 ps (black), and the corresponding maximum X-ray photon energies are 87.30 keV and 321.48 keV in the PIC simulation, a best fit with the synchrotron betatron spectrum. The insets show the energy spectrum of the electrons at the accelerating time.

D. Performance analysis of X-ray communication during re-entry

Although X-ray carriers can be affected during re-entry because of the rarefied atmosphere, increasing the X-ray emitted energy contributes to realizing the uplink communication with a high transmission efficiency.[11,37] In this section, we discussed the X-ray photon transmission model, plasma and atmospheric channel, and photon information efficiency, followed by a description of the theoretical maximum data rate of the X-ray carrier based on the PIC simulation results. Considering the arrangement of our X-ray uplink communication from spacecraft to the ISS of Fig. 1, the amount of optical power focused on the receiver is derived as[38]

$$P_r = \frac{P_t A_r \eta_{fs} \eta_p \eta_r}{\pi(\theta d)^2}, \tag{9}$$

where P_t is the transmitted X-ray power, A_r is the area of the receiver, η_{fs} is the free-space transmission, and η_p and η_r are the transmission of the X-ray carrier through a plasma sheath and the receiver's efficiency. d is the communication distance between spacecraft and the receiver located at ISS. The opening angle of the diverging beam is $\theta = 1.22\lambda/D_t$ (in radian) for a diffraction limited transmitter. What really determines the size of the beam divergence are the optical channel and the pointing jitter.

Previous research[39] has shown that the X-ray signal can be measured and demodulated with only 20 X-ray photons per second detected by a MCP detector, which demonstrates precise timing that allows the recovery of tiny signals from noise; let alone the much higher X-ray photon yields the scheme that we proposed in this paper. In many circumstances, X-ray photons are precious in the space communication due to the large distances involved. Therefore, the data rate is photon-limited. In general, the dimensions of X-ray photons can be any degree of freedom afforded to the communication link, including the time of arrival at a receiver, energy, frequency, and polarization. This means that employing the optimal encoding scheme makes each photon carry more information and then maximizes the photon information efficiency (PIE). For the XCOM system, the L-pulse-position-modulation (PPM) can be used as a simple modulation scheme considering the time of arrival. Each dataset containing n bits of information is transmitted in one of the $L = 2^n$ time slots. For example, with 16-PPM, one photon carries 4 bits of information. Intensity modulation based on different X-ray photon energies would be another similar encoding scheme for the XCOM system with $E = 2^i$ possible energy levels and realize $\log_2 E$ bits of information per photon. Therefore, if the encoding dimensions can be combined, the PIE (in bits per photon) would be enhanced. Although the PIE will be unbound in theory, the limitation in practice arises from the limited numbers of modes per photon (M) depending on the modulation scheme, the thermal noise photon per mode ($N_M = 0.01$ in this paper), and the transmissivity (η_{fs}). The Holevo capacity (upper limit to the amount of information) is given by[40]

$$C = g\left(\eta_{fs} M + (1-\eta_{fs}) N_M\right) - g\left((1-\eta_{fs}) N_M\right), \tag{10}$$

where $g(x) = (1+x)\log_2(1+x) - x\log_2 x$. From the above link equation, the received power can be predicted for a given communication system. Considering a given data rate (R) and modulation schemes, the photon's power detected by the receiver is expressed as[38]

$$P_r = \frac{R E_p}{Q_e C}, \tag{11}$$

where E_p is the photon's energy and Q_e is the quantum efficiency of the receiver.

For a general XCOM system, if a silicon drift detector is used for the X-ray carrier receiver, the typical values[41] of an effective collection area A_r and the detect efficiency η_r are 80 mm^2 and 1, and the quantum efficiency Q_e is almost 0.9. The transmission efficiency of the X-ray carrier through a plasma sheath[23] and the rarefied atmosphere[11] during re-entry is 0.994 and 0.8 based on our previous results. The distance between spacecraft (the X-ray emitter) and ISS (the receiver) is 300 km. The potential application of the laser-plasma X-ray generation scheme would be exploited in blackout communication due to its broadband X-ray energy with extremely low angular distributions ($\theta = 0.04$ rad $\times$ 0.03 rad) and the high photon yields as earlier mentioned, which contributes to the X-ray signal detection by a SDD detector. The emitted power of the X-ray carrier in the scheme is 0.7 W calculated in the PIC simulation. We selected the emitted X-ray energies in the range of 1–100 keV to calculate data rates. As illustrated in Fig. 5, on the one hand, the 8-PPM encoding scheme for the X-ray carrier can reach a higher data rate than 4-PPM at a given X-ray energy. On the other hand, the data rate decreases as the emitted X-ray energy increases. According to the current scheme, the maximum data rate of the X-ray carrier will be up to 20.7 Mbps with the 8-PPM scheme. Because the 8-PPM scheme considers more dimensions (modes) per photon than 4-PPM, the photon information efficiency will be enhanced and then the data rate increases. Moreover, although the information efficiency is related to the number of photons per mode, even for extremely thermal noise levels and more modes per photon, it will not exceed more than a few dozen bits per photon. Therefore, the data rates have no large gap between the 8-PPM and 4-PPM encoding schemes. One can proceed to draw a conclusion that

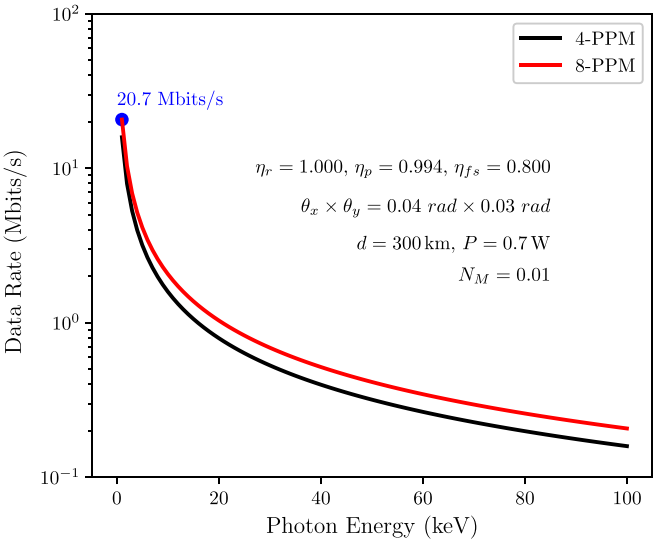

FIG. 5. Data rate of X-ray communication through a plasma sheath during spacecraft re-entry, as a function of the emitted X-ray photon energy based on laser-plasma interaction. The current encoding scheme contains the temporal, energy, and polarization modes per photon.

the data rate of XCOM will be further improved if an effective detect area of the receiver, a monochromatic or narrow X-ray carrier, and the relevant photon information efficiency are optimized as technologies advance.

IV. CONCLUSION

This paper theoretically aims to provide a new route to realize real-time blackout communication encountered during spacecraft re-entry based on the laser-plasma-induced X-ray emission. We performed 2D-PIC simulation to indicate that the modulated laser interaction with the plasma sheath around the surface of supersonic spacecraft could generate the ultra-bright X-ray output with high photon yields, a small angular divergence, and a tunable X-ray energy range in the betatron radiation. The scheme meets the demand of XCOM modulated signal emitted source technology and can provide high-rate, deep-space, low transmit power, and highly secure space-to-space data links. Finally, XCOM system performances during re-entry were estimated to deliver high ($\sim$ Mbps) data rates by considering the transmission model, encoding scheme, and photon information efficiency. Combined with the existing or developed advanced X-ray signal detection methods, this new regime shows a promising applicability for real-time blackout communication encountered during spacecraft re-entry into the planetary atmosphere.

These theoretical results may be helpful for understanding the advantages of XCOM through a plasma sheath, and the novel scheme based on laser-plasma-induced X-ray emission provides a potential approach to mitigate blackout communication during spacecraft re-entry to some extent. However, further investigations are still required to study the modulated X-ray signal source used for XCOM, and the following proof-of-principle experiments will be conducted in the near future.

ACKNOWLEDGMENTS

We acknowledge support from the China Scholarship Council (CSC), the China Postdoctoral Science Foundation (Grant No. 2016M601807), the Postgraduate Research & Practice Innovation Program of Jiangsu Province (Grant No. KYCX17_0257), the Project supported by the Fundamental Research Funds for the Central Universities (Grant No. NP2018408), and the Priority Academic Program Development (PAPD) of Jiangsu Higher Education Institutions. We appreciate the discussion about the EPOCH code which is developed under the UK EPSRC Grant Nos. EP/G054950/1, EP/G056803/1, EP/G055165/1, and EP/M022463/1.

REFERENCES

[1]A. Mecozzi, Nat. Photonics **11**(9), 537–539 (2017).
[2]NASA Technology Roadmaps, "Communication, navigation, and orbital debris tracking and characterization systems," Report No. TA5, 2015, pp. 12–13, see https://www.nasa.gov/sites/default/files/atoms/files/2015_nasa_technology_roadmaps_ta_5_communication_and_navigation_final.pdf.
[3]G. Porter, *See Straight Through Data Center Bandwidth Limitations with X-Rays* (CiteSeer, 2013).
[4]NASA, "Next-generation communications: 'Demonstrating the world's first x-ray communication system'," Report No. FS-2007-10-103-GSFC (TT#7), 2007.
[5]C. Kealhofer, S. M. Foreman, S. Gerlich, and M. A. Kasevich, Phys. Rev. B **86**(3), 035405 (2012).
[6]M. Keidar, M. Kim, and I. Boyd, J. Spacecraft Rockets **45**(3), 445 (2008).
[7]M. P. Bachynski, J. Res. Natl. Bureau Standards Sect. D-Radio Sci. **69**(2), 147 (1965).
[8]X. T. Gao and B. H. Jiang, J. Appl. Phys. **117**(23), 233301 (2015).
[9]L. C. Schroeder and N. D. Akey, J. Spacecraft Rockets **10**(3), 170 (1973).
[10]T. Yusuke, K. Yamada, and T. Abe, J. Spacecraft Rockets **51**(2), 430 (2014).
[11]H. Li, X. B. Tang, S. Hang, Y. P. Liu, and D. Chen, J. Appl. Phys. **121**(12), 123101 (2017).
[12]P. Maine, D. Strickland, P. Bado, M. Pessot, and G. Mourou, IEEE J. Quantum Electron. **24**(2), 398–403 (1988).
[13]T. Tajima and J. M. Dawson, Phys. Rev. Lett. **43**(4), 267 (1979).
[14]E. Esarey, C. B. Schroeder, and W. P. Leemans, Rev. Mod. Phys. **81**(3), 1229 (2009).
[15]K. Liu, R. Y. Chen, S. Khan, and V. J. Sorger, Laser Photonics Rev. **9**(2), 172 (2015).
[16]L. L. Yu, Y. Zhao, L. J. Qian, M. Chen, S. M. Weng, Z. M. Sheng, D. A. Jaroszynski, W. B. Mori, and J. Zhang, Nat. Commun. **7**, 11893 (2016).
[17]Z. Y. Chen and A. Pukhov, Phys. Plasmas **23**(12), 123107 (2016).
[18]L. Winternitz, K. C. Gendreau, M. A. Hasouneh, J. W. Mitchell, W. H. Fong, W. T. Lee, F. Gavriil, and Z. Arzoumanian, "The role of X-rays in future space navigation and communication," in *Proceedings of the 36th Annual Guidance and Navigation Control Conference* (American Astronautical Society, 2013).
[19]Y. Ma, L. M. Chen, N. A. M. Hafz, D. Z. Li, K. Huang, W. C. Yan, J. Dunn, Z. M. Sheng, and J. Zhang, Appl. Phys. Lett. **105**(16), 161110 (2014).
[20]S. Corde, K. T. Phuoc, G. Lambert, R. Fitour, V. Malka, and A. Rousse, Rev. Mod. Phys. **85**(1), 1 (2013).
[21]L. M. Chen, W. C. Yan, D. Z. Li, Z. D. Hu, L. Zhang, W. M. Wang, N. Hafz, J. Y. Mao, K. Huang, Y. Ma, J. R. Zhao, J. L. Ma, Y. T. Li, X. Lu, Z. M. Sheng, Z. Y. Wei, J. Gao, and J. Zhang, Sci. Rep. **3**, 1912 (2013).
[22]T. D. Arber, K. Bennett, C. S. Brady, A. Lawrence-Douglas, M. G. Ramsay, N. J. Sircombe, P. Gillies, R. G. Evans, H. Schmitz, A. R. Bell, and C. P. Ridgers, Plasma Phys. Controlled Fusion **57**(11), 113001 (2015).
[23]Y. P. Liu, H. Li, Y. L. Li, S. Hang, and X. B. Tang, Phys. Plasmas **24**(11), 113507 (2017).
[24]R. Rawhouser, "Overview of the AF avionics laboratory re-entry electromagnetics program," Technical Report No. 19710011627, NASA, Washington, DC, USA, 1970.
[25]S. Poddar and D. Sharma, Optik **126**(24), 5899 (2015).
[26]G. Z. Sun, E. Ott, Y. C. Lee, and P. Guzdar, Phys. Fluids **30**(2), 526 (1987).
[27]W. Lu, M. Tzoufras, C. Joshi, F. S. Tsung, W. B. Mori, J. Vieira, R. A. Fonseca, and L. O. Silva, Phys. Rev. Spec. Top. Accel. Beams **10**(6), 061301 (2007).
[28]H. Mimura, H. Yumoto, S. Matsuyama, and Y. Sano, Appl. Phys. Lett. **90**(5), 051903 (2007).
[29]Y. Suzuki, A. Takeuchi, H. Takano, and H. Takenaka, Jpn. J. Appl. Phys., Part 1 **44**, 1994 (2005).
[30]C. G. Schroer, O. Kurapova, and J. Patommel, Appl. Phys. Lett. **87**(12), 124103 (2005).
[31]T. W. Huang, C. T. Zhou, H. Zhang, S. Z. Wu, B. Qiao, X. T. He, and S. C. Ruan, Appl. Phys. Lett. **110**(2), 021102 (2017).
[32]K. Iwamoto, T. Nakao, T. Ito, T. Sano, T. Ishii, K. Shibata, M. Ueno, S. Ohta, H. Komatsu, T. Arak, Y. Kobayashi, and H. Sawada, "Small optical inter-satellite communication system for small and micro satellites," Proc. SPIE **10096**, 100960T-7 (2017).
[33]S. Fourmaux, S. Corde, K. T. Phuoc, P. M. Leguay, S. Payeur, P. Lassonde, S. Gnedyuk, G. Lebrun, C. Fourment, V. Malka, S. Sebban, A. Rousse, and J. C. Kieffer, New J. Phys. **13**(3), 033017 (2011).
[34]J. D. Jackson, *Classical Electrodynamics* (Wiley, New York, 1975).
[35]A. Rousse, K. T. Phuoc, R. Shah, A. Pukhov, E. Lefebvre, V. Malka, S. Kiselev, F. Burgy, J. P. Rousseau, D. Umstadter, and D. Hulin, Phys. Rev. Lett. **93**(13), 135005 (2004).
[36]V. Horný, J. Nejdl, M. Kozlová, M. Krůs, K. Boháček, V. Petržílka, and O. Klimo, Phys. Plasmas **24**(6), 063107 (2017).
[37]S. Hang, Y. P. Liu, H. Li, X. B. Tang, and D. Chen, Nucl. Instrum. Methods Phys. Res., Sect. A **887**, 18 (2018).
[38]A. K. Majumdar, *Advanced Free Space Optics (FSO): A Systems Approach* (Springer, 2014), p. 186.
[39]C. Kealhofer, "Ultrafast X-ray point source for space-based communication" (2010), see https://web.stanford.edu/group/scpnt/pnt/PNT10/student_posters/SCPNT%202010%20Foreman.pdf.
[40]V. Giovannetti, S. Guha, S. Lloyd, L. Maccone, J. H. Shapiro, and H. P. Yuen, Phys. Rev. Lett. **92**(2), 027902 (2004).
[41]B. Beckhoff, B. Kanngießer, N. Langhoff, R. Wedell, and H. Wolff, *Handbook of Practical X-ray Fluorescence Analysis* (Springer Science and Business Media, 2007).